Available online at www.sciencedirect.com
SCIENCE DIRECT®
Journal of Solid State Chemistry 177 (2004) 1137–1145
JOURNAL OF SOLID STATE CHEMISTRY
http://elsevier.com/locate/jssc

Evidence for the two-dimensional hybridization in $Na_{0.79}CoO_2$ and $Na_{0.84}CoO_2$

H. Nakatsugawa* and K. Nagasawa

Division of Materials Science and Engineering, Graduate School of Engineering, Yokohama National University, 79-5 Tokiwadai, Hodogaya Ward, Yokohama 240-8501, Japan

Received 13 July 2003; received in revised form 10 October 2003; accepted 26 October 2003

Abstract

The electron density distributions of $Na_{0.79}CoO_2$ and $Na_{0.84}CoO_2$ have been obtained by the maximum entropy method and the Rietveld analysis using powder X-ray diffraction data at room temperature. In the Rietveld refinement, there are good agreement between $x = 0.79(4)$ and $x = 0.84(9)$, except for (008) and (108) peaks. The deviations of the two reflections are very large relative to those of other reflections, and the change in X-ray diffraction data is clearer than that in neutron diffraction data. This indicates that electron density distributions in Na_xCoO_2 are slightly modulated with increasing x. In fact, there are an obvious overlapping of the electron density between Co and O due to the Co–O hybridization in the CoO_2 layer, but the two-dimensional networks in the electron densities of $x = 0.84(9)$ are suppressed by the existence of the O–O network on (008) plane. This is direct evidence of decrease of two-dimensional hybridization in the CoO_2 layer with increasing a sodium content.

Keywords: Na_xCoO_2; Sodium content; CoO_2 layer; O–O network; Hybridization; Maximum entropy method

1. Introduction

Recently, a layered cobalt oxide Na_xCoO_2 have been known as a promising candidate for thermoelectric materials because of its large thermoelectric power (S) coexisting with low electric resistivity (ρ) [1]. The carrier concentration has been found to be much higher in this system, i.e., the order of $10^{21}-10^{22}$ cm^{-3}, than in some known thermoelectric materials such as Bi_2Te_3 and PbTe [2]. The large value reported for S of $Na_{0.5}CoO_2$, i.e., $S > 50$ μV/K at room temperature, is difficult to be understood within the framework of conventional one-electron picture [3]. A recent result of heat capacity measurements [4] revealed that the effective mass of the carrier (holes) of this compound was as large as those of strongly correlated electrons. Terasaki [3] suggested that both the strong electron correlation and the spin sate in Co site play a crucially important role in the enhancement of S. The magnetic susceptibility (χ) of polycrystalline sample of $Na_{0.5}CoO_2$ was successfully explained by the coexistence of Co^{3+} (low spin (LS): t_{2g}^6) and Co^{4+} (LS: t_{2g}^5) [5]. Koshibae et al. [6] established a theory generalizing the Heikes' formula [7] and suggested that the observed large magnitude of S in Na_xCoO_2 would be originated from both the large degeneracy of Co species of various spin states and the strong correlation of $3d$ electrons. It was concluded that the LS state in Co site is a key factor for the large Seebeck coefficient.

The structure of the material is of a layer type consisting of CdI_2-type CoO_2 conducting layers which are made of edge-shared CoO_6 octahedra and inter-layers of Na^+ ions alternately stacked along the c-axis. The sodium ions are intercalated in trigonal prismatic or octahedral coordination of oxygen atoms and are mobile even at room temperature, but the ionic conductivity is much smaller than the electronic conductivity in the CoO_2 layers. Fouassier et al. [8] have reported that Na_xCoO_2 has four distinct bronze-type phases, i.e., α (O3-type structure), α' (O′3-type structure), β (P3-type structure), and γ (P2-type structure), and the difference among these four phases is in the stacking sequence of oxygen atom layers. The neutron diffraction investigation [9] of $Na_{0.74}CoO_2$ has shown that the material has a hexagonal γ phase (space

*Corresponding author. Fax: +81-45-331-6593.
E-mail address: naka@ynu.ac.jp (H. Nakatsugawa).

0022-4596/$ - see front matter © 2003 Elsevier Inc. All rights reserved.
doi:10.1016/j.jssc.2003.10.035

group: $P6_3/mmc$, No. 194) and that there are two types of Na^+ sites, i.e., $2b(0,0,\frac{1}{4})$ and $2d(\frac{2}{3},\frac{1}{3},\frac{1}{4})$, with different occupancies. The $2d$ site is in a trigonal prismatic environment, while the $2b$ site has neighboring Co ions above and below the trigonal prism of the oxygen atom, which should cause the difference in the occupancy. Such a disordered structure also should cause a low thermal conductivity, i.e., 20 mW/cm K at room temperature, which was attributed to the short phonon mean-free path arising from the Na deficiency [10].

Na_xCoO_2 is known to show a wide range of Na nonstoichiometry within $0.5 \leqslant x \leqslant 1.0$ [8], where the valence of Co changes $Co_x^{3+}Co_{1-x}^{4+}$ in accordance with Na^+ content x. Since Na is volatile, it has been recognized that the control of x is difficult for Na_xCoO_2 by a conventional solid-state reaction method [11]. Recently, however, Motohashi et al. [12,13] established an unconventional method named rapid heat-up technique to precisely control a sodium content in Na_xCoO_2 samples, in which Na evaporation during the synthesis is minimized. For thus prepared samples of $Na_{0.75}CoO_2$ exhibit $S \simeq 120\ \mu V/K$ at room temperature [12], and show a magnetic transition of the second-order below 22 K [13]. These features strongly indicate the appearance of an unusual electronic state that may be attributed to the strongly correlated electrons in $Na_{0.75}CoO_2$. Furthermore, Tojo et al. [14] measured the heat capacity of $Na_{0.75}CoO_2$ and found first-order phase transitions at 288.7, 296.3, and 302.1 K. The X-ray diffraction patterns in $Na_{0.75}CoO_2$ at 123 and 333 K indicate that the most probable mechanism of the phase transition around room temperature is the occurrence of some kind of ordering in Na^+ layers [14]. Although a large number of studies have been made on the strongly correlated electron system in the CoO_2 layers, little is known about a relationship between the CoO_2 layers and the Na^+ layers. Thus, a further investigation is needed to confirm these clearly. From this point of view, the magnetic properties, the parameters of the crystal structure, and the electron density distributions visualized by a combination of the maximum entropy method (MEM) and a Rietveld refinement [15,16] in Na-richer samples by a conventional solid-state reaction method have been investigated in the present study.

2. Experiment

Two polycrystalline Na-richer samples of Na_xCoO_2 were prepared by a conventional solid-state reaction method. Starting powders of Na_2CO_3 and Co_3O_4 were mixed in molar ratios of Na : Co = (i) 0.909 : 1 and (ii) 0.948:1, and calcined each sample at 1123 K for 12 h in air. Then, the samples were reground, pressed into pellets and sintered at 1173 K for 12 h in air. Finally, the pellets were cooled in the furnace to room temperature at a rate of 1 K/min. The resulting powder sample was characterized by X-ray diffraction (XRD), neutron diffraction (ND), and inductively coupled plasma atomic-emission spectrometry (ICP-AES) analysis. The XRD and ND patterns showed good identification of the samples as the γ phase, and there was no indication of the presence of other prototypes or residual raw materials. The molar ratio of metal ions in the two samples for Na_xCoO_2 was determined to be Na : Co = (i) 0.79(4) : 1 and (ii) 0.84(9):1 by the ICP-AES analysis. This indicates that about 12–14% Na^+ ions are missing from the initial compositions. The weight loss due to decomposition of the raw materials starts from about 773 K and continues up to 1023 K, where Na_xCoO_2 phase formation is completed above 1023 K, that is, the weight loss between 723 and 1023 K is too large (7–8%) to be explained only with decarbonation of the raw materials (5–6%) [12].

The XRD measurement was carried out using a JEOL JDX-3530 X-ray diffractometer system at room temperature. The powder sample is pressed on a glass plate, mounted vertically on the sample table and diffraction patterns are recorded using Cu$K\alpha$ ($\lambda = 1.542$ Å) radiation. The XRD data are collected in 2θ range from 10° to 90° in steps of 0.02° using a scintillation detector. The ND measurement was carried out at room temperature using the HERMES powder neutron diffractometer installed on T1-3 port of JRR-3M reactor in the Japan Atomic Energy Research Institute (JAERI), Tokai Establishment [17]. An incident neutron wavelength $\lambda =$ 1.8207 Å was obtained from a Ge(311) monochromater. The ND data were collected on thoroughly ground powders by a multiscanning mode in the 2θ range from 10° to 153° with a step width of 0.10°.

The structure determination of Na_xCoO_2 was analyzed using the Rietveld analysis program, RIETAN-2000 [18]. The electron density distributions at room temperature were visualized by an elaborate method, which are combination of the MEM and the Rietveld refinement of the XRD data [15,16]. The technique has been successfully applied to the structure studies of fullerene compounds [19,20], intermetallic compounds [21], manganites [22], etc. Magnetic susceptibility (χ) was measured between 10 and 330 K using a commercial apparatus from Quantum Design MPMS superconducting quantum interference device (SQUID) magnetometer.

3. Results and discussion

3.1. Crystal structures at room temperature

The powder XRD data showed that the samples of $Na_{0.79}CoO_2$ and $Na_{0.84}CoO_2$ were single phase and had the P2-type hexagonal structure at room temperature.

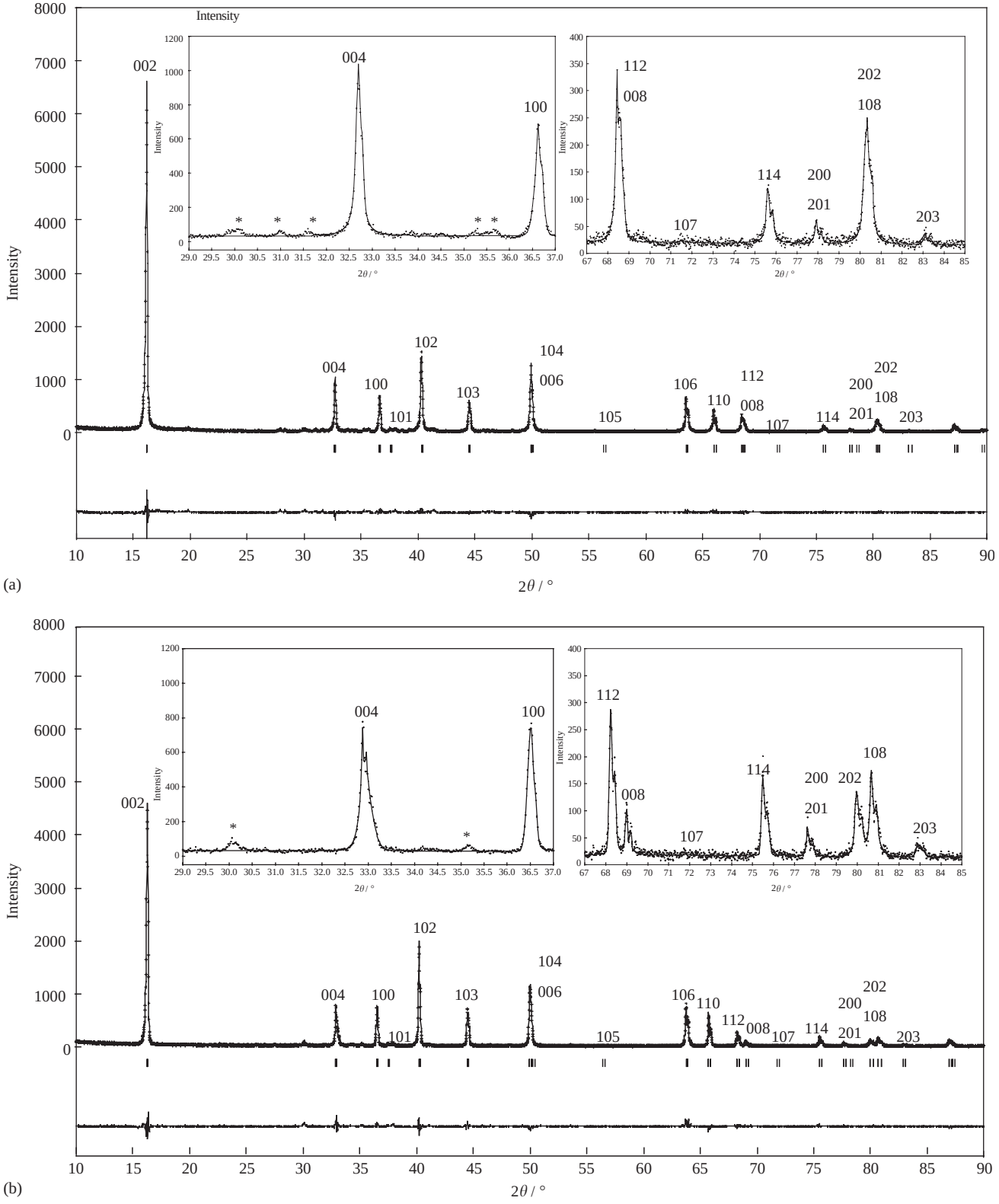

Fig. 1. Rietveld fitting of powder XRD data for: (a) $Na_{0.79}CoO_2$ and (b) $Na_{0.84}CoO_2$ at room temperature. Tick marks represent the positions of possible Bragg reflections. The insets show the reflections in the 2θ ranges ($29°-37°$ and $67°-85°$). The peaks for unreacted Na_2CO_3 are marked with '$*$'. The difference curve between observed and calculated intensities is shown at the bottom of the figure.

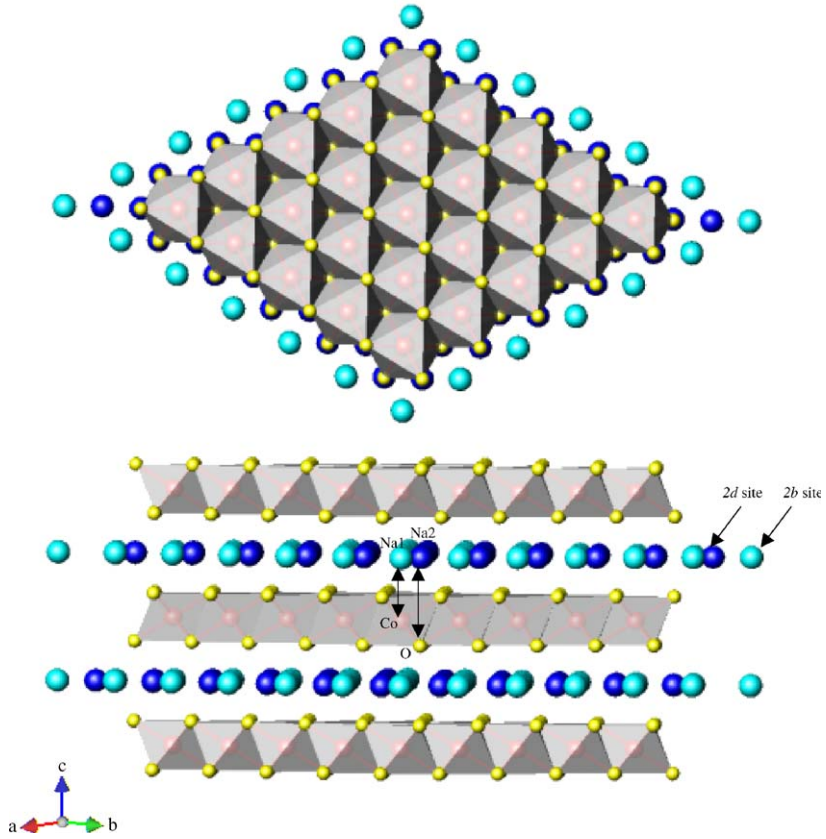

Fig. 2. Crystal structure of γ-Na_xCoO_2 which has the P2-type hexagonal structure (space group: $P6_3/mmc$, No. 194) at room temperature.

Although four space groups, i.e., $P6_322$ (No. 182), $P6_3mc$ (No. 186), $P\bar{6}2c$ (No. 190) and $P6_3/mmc$ (No. 194), were possible for γ-Na_xCoO_2, the highest symmetry $P6_3/mmc$-type space group (No. 194) was chosen as it described the refined structure equally [9]. In Figs. 1(a) and (b), the results of the Rietveld refinement are shown with a tiny trace of an unreacted Na_2CO_3 as marked by '$*$' for $Na_{0.79}CoO_2$ and $Na_{0.84}CoO_2$, respectively. In the present analysis we assumed that Na1 and Na2 ions occupy $2b(0,0,\frac{1}{4})$ and $2d(\frac{2}{3},\frac{1}{3},\frac{1}{4})$ sites, respectively. Fig. 2 shows the schematic representation of crystal structure for γ-Na_xCoO_2. The weighted profile reliability factors of the Rietveld refinement as a pre-analysis for the MEM, R_{wp}, were 16.82% for $x = 0.79(4)$ and 16.83% for $x = 0.84(9)$. The reliability factors based on the integrated intensities, R_I, were 4.68% and 5.20%, respectively. There are good agreement between the results of the Rietveld refinement, except for two peaks, i.e., (008) ($2\theta \simeq 68°-69°$) and (108) ($2\theta \simeq 80°-81°$). It should be noted that the (112) and (202) reflections deviate to low 2θ angle side, but the (008) and (108) reflections deviate to high 2θ angle side with increasing x.

The powder ND data also showed that the specimens of $Na_{0.79}CoO_2$ and $Na_{0.84}CoO_2$ had the P2-type hexagonal structure which was assigned to $P6_3/mmc$ (No. 194) at room temperature. In Figs. 3(a) and (b), the results of the Rietveld refinement in the 2θ range from 75° to 105° are shown for two samples. Refined structure parameters, final reliability factors, and Goodness of fits are given in Table 1 together with the selected interatomic distances and bond angles. Sodium ions at $2b$ and $2d$ sites have a large thermal parameter B, implying disorder of sodium ions around these sites. There are two kinds of prisms, i.e., $Na1O_6$ and $Na2O_6$ prisms [23]. The $Na1O_6$ prism at $2b$ site shares two sets of three oxygen atoms with upper and lower one CoO_6 octahedara, respectively. On the other hand, the $Na2O_6$ prism at $2d$ site shares two sets of three oxygen atoms with upper and lower three CoO_6 octahedara, respectively. Judging from the ionic radius of Na^+ for six coordinations (1.02 Å) [24], the Na^+ ions cannot fully occupy the adjacent $2b$ and $2d$ sites because of the Na1–Na2 distances ($\simeq 1.63$ Å). Thus, the sodium ions are randomly distributed at the $2b$ and $2d$ sites with different occupancies, i.e., ($2b: 0.286 + 2d: 0.508$) for $Na_{0.79}CoO_2$ and ($2b: 0.302 + 2d: 0.547$) for $Na_{0.84}CoO_2$ which are in good agreement with that obtained by the ICP-AES chemical analysis. The observed Co–O distances and O–Co–O bond angles are comparable with those reported in γ-$Na_{0.7}CoO_2$ [8].

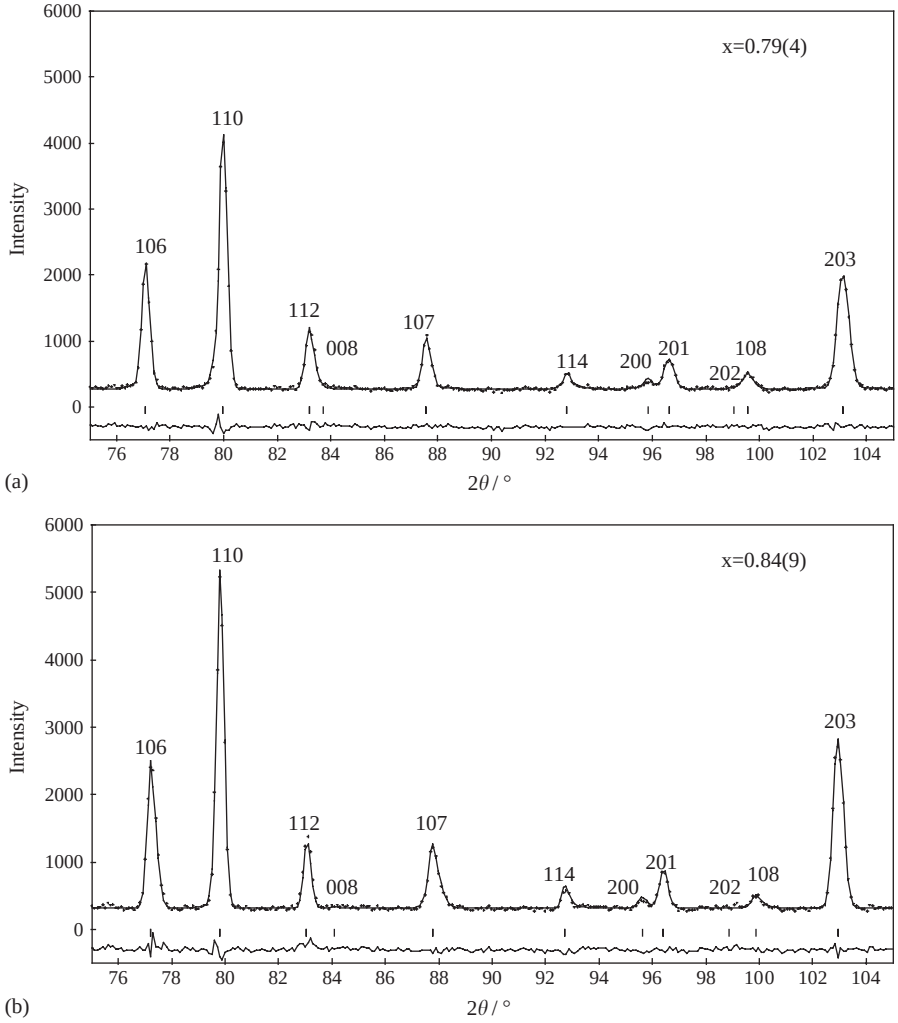

Fig. 3. Rietveld fitting of powder ND data in the 2θ range from 75° to 105° for: (a) $Na_{0.79}CoO_2$ and (b) $Na_{0.84}CoO_2$ at room temperature, respectively. Tick marks represent the positions of possible Bragg reflections. The difference curve between observed and calculated intensities is shown at the bottom of the figure.

3.2. MEM electron density distributions

The number of observed XRD structure factors derived in the Rietveld analysis at room temperature were 24 for each set of data, which were used for further MEM analysis. In the present analysis, total electrons in the unit cell were fixed to be $103.5e$ for $Na_{0.79}CoO_2$ and $104.7e$ for $Na_{0.84}CoO_2$, respectively. Following the Rietveld analysis, the MEM analysis was carried out with a computer program, MEED [25], using $50 \times 50 \times 100$ pixels to ensure good spatial resolution. The total of 24 independent reflections in the range of $\sin\theta/\lambda < 0.46$ Å were used. The reliability factors of the MEM based on the structure factors, R_F, were 4.61% for $x = 0.79(4)$ and 4.96% for $x = 0.84(9)$, respectively. R_F is expressed as $R_F = \sum|F_{obs} - F_{MEM}|/\sum|F_{obs}|$, where F_{obs} is obtained by structural refinement and F_{MEM} is calculated from electron density obtained by the MEM. In the MEM imaging, any kind of deformation of electron densities is allowed as long as it satisfies the symmetry requirements. This method enables us to visualize more detailed features included in the observed data like the bonding electron distribution associated with hybridized orbitals.

In Figs. 4(a) and (b), the three-dimensional representation of the MEM electron densities by an equi-contour surface of $2.5e/Å^3$ and $2.0e/Å^3$ for samples of $x = 0.79(4)$ and 0.84(9), respectively. In these figures, there found to be the O–O network on (008) plane due to the O $2p$–O $2p$ orbital hybridization at an equi-contour surface of $2.0e/Å^3$ for $x = 0.84(9)$, while no bonding between oxygen ions is observed at an equi-contour surface of $2.0e/Å^3$ for $x = 0.79(4)$. Figs. 5(a) and (b) show the MEM electron densities by an equi-contour surface of $1.8e/Å^3$ for $x = 0.79(4)$ and that of $1.5e/Å^3$ for $x = 0.84(9)$, respectively. In these figures, there are

Table 1
Structural parameters, final reliability factors and goodness of fits for $Na_{0.79}CoO_2$ and $Na_{0.84}CoO_2$ at room temperature

Atom	Site		$x=$ 0.79(4)	$x=$ 0.84(9)
Na1	$2b(0,0,\frac{1}{4})$	Atoms/formula unit	0.28(5)	0.30(2)
		B(Å^2)	0.763(9)	1.07(1)
Na2	$2d(\frac{2}{3},\frac{1}{3},\frac{1}{4})$	Atoms/formula unit	0.50(8)	0.54(7)
		B(Å^2)	0.763(9)	1.07(1)
Co	$2a(0,0,0)$	Atoms/formula unit	1.0	1.0
		B(Å^2)	0.0631(7)	0.167(6)
O	$4f(\frac{1}{3},\frac{2}{3},z)$	Atoms/formula unit	2.0	2.0
		z	0.0898(4)	0.0902(1)
		B(Å^2)	0.312(2)	0.351(7)
	Lattice parameters	a(Å)	2. 831(5)	2. 836(2)
		c(Å)	10.90(7)	10.86(8)
	Reliability factors	R_{wp}(%)	6.96	7.26
		R_I(%)	3.79	3.59
		R_F(%)	3.50	3.39
	Goodness of fit	$S=R_{wp}/R_e$	1.37	1.55
	Interatomic distances	Co–O(Å)	1.906(1)	1.908(5)
		Na1–Na2(Å)	1.634(8)	1.637(5)
	Bond angles	O–Co–O(deg)	95.93(8)	95.98(1)

Space group: $P6_3/mmc$, No. 194. Selected Co–O distances, Na1–Na2 distances and O–Co–O bond angles for both samples are also tabulated.

an obvious overlapping of the electron density between Co and O due to the Co–O hybridization in the CoO_2 layer, but two-dimensional networks in the MEM electron densities of $x=0.84(9)$ are suppressed by the existence of the O–O network on (008) plane. This is the direct observation of decrease of the two-dimensional hybridization in the CoO_2 layer with increasing a sodium content.

3.3. Magnetic properties

Fig. 6 shows the plots of the inverse magnetic susceptibility $(\chi-\chi_0)^{-1}$ for the specimens of $x=0.79(4)$ and 0.84(9) versus temperature T measured under the external magnetic field of 5000 Oe, where χ_0 is the contribution of temperature-independent magnetic susceptibility. The observed temperature dependence of magnetic susceptibility χ was similar to the Curie–Weiss and to those reported for $Na_{0.5}CoO_2$ by Ray et al. [5]. The $\chi-T$ curve can be expressed as: $\chi=\chi_0+C/(T-\Theta)$, where C is the Curie constant and Θ is the paramagnetic Curie temperature. A large deviation was found below 30 K, which may imply the increase of the magnetic interaction. Thus, we used the data at temperatures higher than 30 K, and the results of the fitting is shown as solid lines in Fig. 6. The values of the parameters obtained are $\chi_0=0.18(5)\times10^{-3}$ emu/mol, $C=0.0794(0)$ emu K/mol, and $\Theta=-74.8(7)$ K for $x=0.79(4)$, and $\chi_0=0.15(5)\times10^{-3}$ emu/mol, $C=0.113(7)$ emu K/mol, and $\Theta=-96.8(8)$ K for $x=0.84(9)$, respectively. The negative value of Θ suggests an antiferromagnetic interaction. In fact, some negative values were also reported for Θ's of γ-Na_xCoO_2 in previous works [5,13,14,23].

In Na_xCoO_2, the magnitude of the formal valence of Co $2a$ site can be interpreted in terms of the coexistence of Co^{3+} and Co^{4+} ions, i.e., $[Na^+]_x[Co^{3+}]_x[Co^{4+}]_{1-x}[O^{2-}]_2$. If both cobalt ions are in the LS state [5], only the Co^{4+} spin ($S=\frac{1}{2}$) is responsible for the magnetic susceptibility. Thus, the effective magnetic moment expected from only localized $S=\frac{1}{2}$ spin is $\mu_{eff}=2\sqrt{S(S+1)}\mu_B=2\sqrt{0.25x^2-x+0.75}\ \mu_B$, where $\mu_{eff}=0.656\ \mu_B$ for $x=0.79(4)$ and $\mu_{eff}=0.570\ \mu_B$ for $x=0.84(9)$. From the Curie constant C, however, the effective magnetic moment μ_{eff} becomes 0.796(8) μ_B for $x=0.79(4)$ and 0.953(8) μ_B for $x=0.84(9)$, respectively. This discrepancy is eliminated by assuming that Co^{4+} ions are in the LS and the intermediate spin (IS) states simultaneously. If the population ratio at the Co $2a$ site is given by LS Co^{3+} : LS Co^{4+} : IS $Co^{4+}=x:1-x-y:y$, the effective magnetic moment is estimated to be $\mu_{eff}=2\sqrt{0.25x^2-x+0.75+y^2+(2-x)y}\,\mu_B$, i.e., $\mu_{eff}=0.796\ \mu_B$ for $Na_{0.79}[LS\ Co^{3+}]_{0.79}[LS\ Co^{4+}]_{0.17}[IS\ Co^{4+}]_{0.04}O_2$ and $\mu_{eff}=0.953\ \mu_B$ for $Na_{0.84}[LS\ Co^{3+}]_{0.84}[LS\ Co^{4+}]_{0.04}[IS\ Co^{4+}]_{0.12}O_2$, respectively. This means that the IS Co^{4+} in the population ratio at the $2a$ site increase with increasing a sodium content.

4. Conclusion

In the Rietveld refinement, there are good agreement between $x=0.79(4)$ and 0.84(9), except for (008) and (108) peaks. The deviations of the two reflections are very large relative to those of other reflections, and the change in XRD data is clearer than that in ND data. This means that electron density distributions in Na_xCoO_2 are slightly modulated with increasing x. In fact, there found to be the O–O network on (008) plane due to the O $2p-$O $2p$ orbital hybridization at an equi-contour surface of $2.0e/Å^3$ for $x=0.84(9)$, while no bonding between oxygen ions is observed at an equi-contour surface of $2.0e/Å^3$ for $x=0.79(4)$. In addition, the MEM electron densities by an equi-contour surface of $1.8e/Å^3$ for $x=0.79(4)$ and that of $1.5e/Å^3$ for $x=0.84(9)$ indicate that there are an obvious overlapping of the electron density between Co and O due to the Co–O

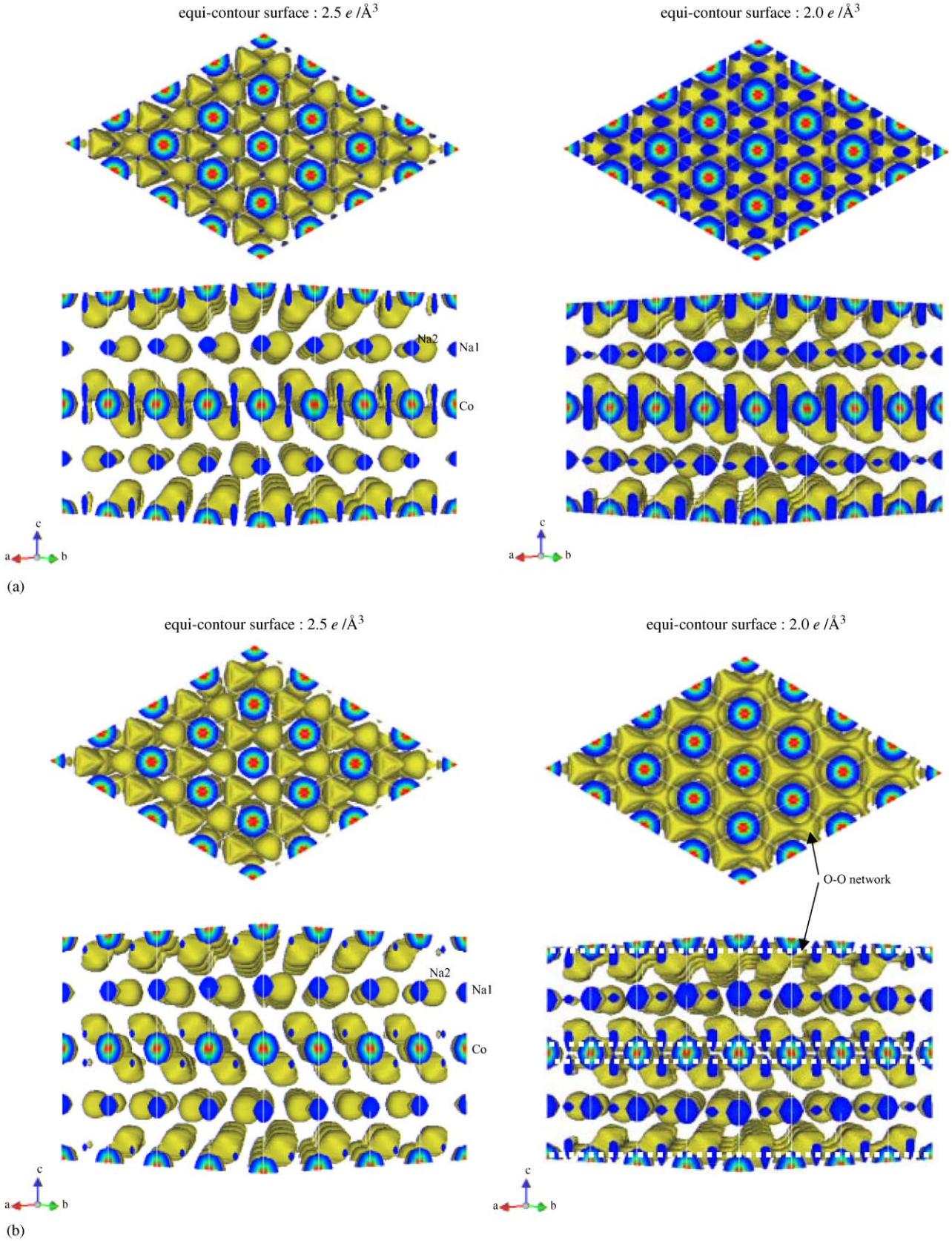

Fig. 4. Three-dimensional representation of the MEM electron densities by an equi-contour surface of $2.5e/Å^3$ and $2.0e/Å^3$ for samples of: (a) $x = 0.79(4)$ and (b) $x = 0.84(9)$ at room temperature, respectively. The dotted lines represent the O–O network on (008) plane.

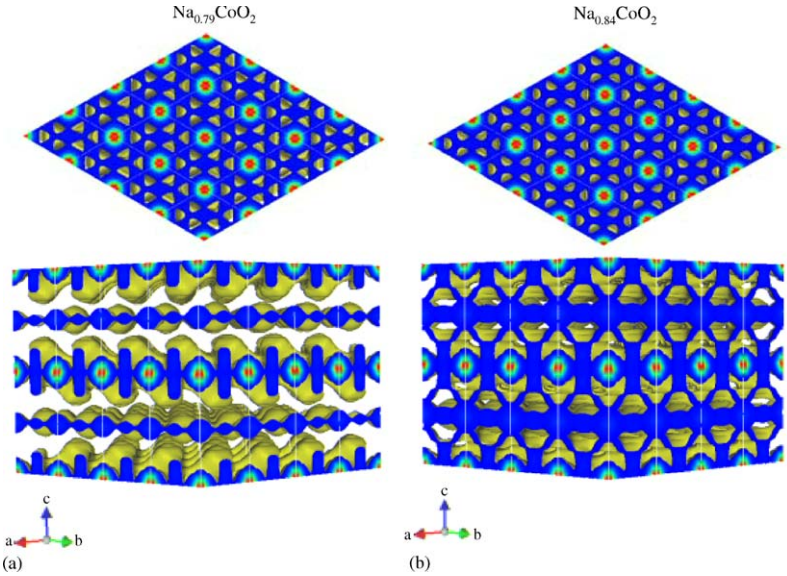

Fig. 5. Three-dimensional representation of the MEM electron densities by an equi-contour surface of: (a) $1.8e/Å^3$ for $x = 0.79(4)$ and that of (b) $1.5e/Å^3$ for $x = 0.84(9)$ at room temperature, respectively.

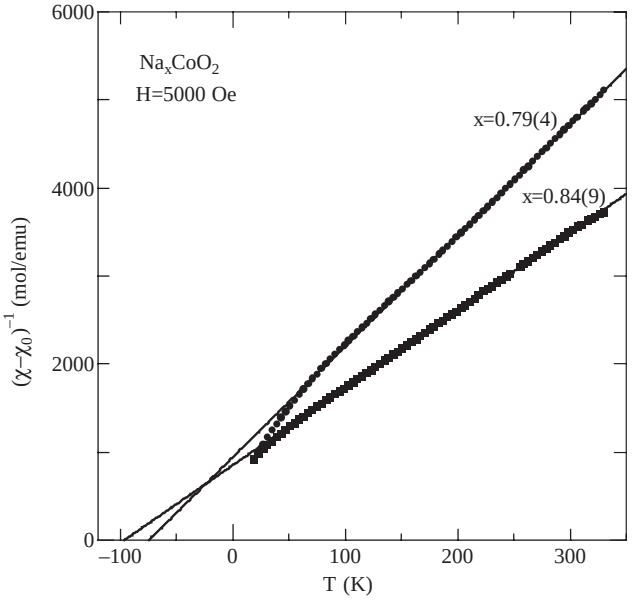

Fig. 6. Temperature dependence of inverse magnetic susceptibility $(\chi - \chi_0)^{-1}$ for the specimens of $x = 0.79(4)$ (solid circles) and $x = 0.84(9)$ (solid squares) measured under the external magnetic field of 5000 Oe, where χ_0 is the contribution of temperature-independent magnetic susceptibility.

hybridization in the CoO_2 layer. Nevertheless, two-dimensional networks in the MEM electron densities of $x = 0.84(9)$ are suppressed by the existence of the O–O network on (008) plane. This is the direct evidence of decrease of the two-dimensional hybridization in the CoO_2 layer with increasing a sodium content. The spin states of Co^{4+} ions at $2a$ sites are in the LS and the IS states, and the IS Co^{4+} increase with increasing x. This indicates that spin states of Co^{4+} ions change from LS (t_{2g}^5) to IS $(t_{2g}^4 e_g^1)$ state. As a result, the two-dimensional hybridization between O2p and Cot$_{2g}$ in the CoO_2 layer decreases with increasing x.

Acknowledgments

We are grateful to A. Tobo for her help in the neutron powder experiment. The authors are grateful to the Kanagawa High-Technology Foundation for inductively coupled plasma atomic-emission spectrometry analysis data. The SQUID magnetometer in Ecotechnology System Laboratory, Yokohama National University, was used. This work was supported by CASIO foundation for the promotion of science, Yazaki foundation for the promotion of science and engineering, and Yokohama manufacturers association foundation.

References

[1] I. Terasaki, Y. Sasago, K. Uchinokura, Phys. Rev. B 56 (1997) R12685.
[2] G. Mahan, B. Sales, J. Sharp, Phys. Today 50 (1997) 42.
[3] I. Terasaki, in: Proceedings of the 18th International Conference on Thermoelectrics (ICT1999), Baltimore, MD, August 29–September 2, 1999, IEEE, Piscataway, 2000, pp. 569–576.
[4] Y. Ando, N. Miyamoto, K. Segawa, T. Kawata, I. Terasaki, Phys. Rev. B 60 (1999) 10580.
[5] R. Ray, A. Goshray, K. Goshray, S. Nakamura, Phys. Rev. B 59 (1999) 9454.
[6] W. Koshibae, K. Tsutsui, S. Maekawa, Phys. Rev. B 62 (2000) 6869.
[7] R.R. Heikes, R.W. Ure Jr., Thermoelectricity: Science and Engineering, Interscience, New York, 1961.

[8] C. Fouassier, G. Matejka, J.-M. Reau, P. Hagenmuller, J. Solid State Chem. 6 (1973) 532.
[9] R.J. Balsys, R.L. Davis, Solid State Ionics 93 (1996) 279.
[10] K. Takahata, Y. Iguchi, D. Tanaka, T. Itoh, I. Terasaki, Phys. Rev. B 61 (2000) 12551.
[11] T. Kawata, Y. Iguchi, T. Itoh, K. Takahata, I. Terasaki, Phys. Rev. B 60 (1999) 10584.
[12] T. Motohashi, E. Naujalis, R. Ueda, K. Isawa, M. Karppinen, H. Yamauchi, Appl. Phys. Lett. 79 (2001) 1480.
[13] T. Motohashi, R. Ueda, E. Naujalis, T. Tojo, I. Terasaki, T. Atake, M. Karppinen, H. Yamauchi, Phys. Rev. B 67 (2003) 064406.
[14] T. Tojo, H. Kawaji, T. Atake, Phys. Rev. B 65 (2002) 0521105.
[15] M. Takata, B. Umeda, E. Nishibori, M. Sakata, Y. Saito, M. Ohno, H. Shinohara, Nature 377 (1995) 46.
[16] M. Takata, E. Nishibori, B. Umeda, M. Sakata, E. Yamamoto, H. Shinohara, Phys. Rev. Lett. 78 (1997) 3330.
[17] K. Ohoyama, T. Kanouchi, K. Nemoto, M. Ohashi, T. Kajitani, Y. Yamaguchi, Jpn. J. Appl. Phys. 37 (1998) 3319.
[18] F. Izumi, T. Ikeda, J. Crystallogr. Soc. Jpn. 42 (2000) 516.
[19] M. Takata, E. Nishibori, M. Sakata, M. Inakuma, E. Yamamoto, H. Shinohara, Phys. Rev. Lett. 83 (1999) 2214.
[20] C.-R. Wang, T. Kai, T. Tomiyama, T. Yoshida, Y. Kobayashi, E. Nishibori, M. Takata, M. Sakata, H. Shinohara, Nature 408 (2000) 426.
[21] Y. Kubota, M. Takata, M. Sakata, T. Ohba, K. Kifune, T. Tadaki, J. Phys.: Condens. Matter 12 (2000) 1253.
[22] M. Takata, E. Nishibori, K. Kato, M. Sakata, Y. Moritomo, J. Phys. Soc. Jpn. 68 (1999) 2190.
[23] Y. Ono, R. Ishikawa, Y. Miyazaki, T. Kajitani, J. Phys. Soc. Jpn. 70 (Suppl. A) (2001) 235.
[24] R.D. Shannon, C.T. Prewitt, Acta Crystallogr. 25 (1969) 925.
[25] S. Kumazawa, Y. Kubota, M. Takata, M. Sakata, Y. Ishibashi, J. Appl. Crystallogr. 26 (1993) 453.